A simple MHD model for coupling poloidal manifolds to breeder units in liquid metal blankets

L. Bühler [*], C. Mistrangelo

Karlsruhe Institute of Technology (KIT), P.O. Box 3640, 76021 Karlsruhe, Germany

ARTICLE INFO

ABSTRACT

An efficient hybrid model has been developed for prediction of magnetohydrodynamic pressure drop in electrically couple manifolds of liquid metal blankets and flow partitioning in breeder units. The tool combines global mass conservation and pressure drop correlations with detailed 3D simulations. When applied to a TBM-like geometry, the model reveals strong electromagnetic coupling with increased flow in BUs is near both ends of the module, while weak coupling with almost no flow is found in BUs in the middle of the module. The method is very efficient and it applies for a large number of BUs as foreseen in a DEMO design. It will be applied in future to determine the optimum position of the baffle plates in manifolds that guarantees uniform flow partitioning in all breeder units.

1. Introduction

In the water-cooled lead lithium (WCLL) blanket currently under investigation in Europe as reference liquid metal concept (see Fig. 1), liquid lead lithium (PbLi) functions as tritium breeder, neutron multiplier and heat carrier. The heat is removed by cooling tubes immersed in the liquid metal that is confined in a large number of breeding units (BUs). For purification and extraction of tritium it is required to circulate the liquid metal slowly to ancillary facilities. The movement of the electrically conducting alloy across the strong plasma-confining magnetic field induces electric currents which are responsible for electromagnetic Lorentz forces that modify the flow pattern and give rise to magnetohydrodynamic pressure drop. For a reasonable performance of the blanket system it is required that each BU receives sufficient fresh PbLi from the manifolds to avoid local accumulation of tritium. Therefore a good understanding of the flow partitioning in BUs and pressure drop in blanket system is required.

Previous analyses and experiments for a helium-cooled lead lithium (HCLL) test blanket module (TBM) for ITER revealed that the major fraction of pressure drop originates from the manifolds, where liquid metal velocities are high and where feeding and draining sections are electrically coupled via leakage currents across electrically conducting common walls [1]. Moreover, it has been found that the manifolds play a decisive role for flow partitioning among BUs [2]. A major result from those investigations is that non-uniform flow distribution is to be expected with considerably higher flow rates in BUs at both ends of the module and reduced flow in central units if manifolds are not designed

in a proper way. Since the current design of WCLL manifolds is quite similar to the one foreseen for HCLL blanket modules, flow partitioning will be a major issue as well and has to be investigated in sufficient detail.

While the design of the WCLL TBM for ITER consists of only 8 BUs per column, the current concept for a DEMO reactor foresees a much larger number of BUs stacked along the poloidal x direction around the fusion plasma (Fig. 1). A full numerical description of the entire blanket segment with the large number N of BUs is not possible with available computational resources. For that reason, the present work aims at defining a physical model that allows determining efficiently flow distribution and pressure drop in the entire blanket module. The model described in the following is based on a number of selected 3D numerical simulations for determining pressure drop correlations in typical blanket elements (single BUs and fractions of manifolds). The results are then assembled in a global model that determines the overall behavior of the full blanket segment. Since details of the manifold are still not completely defined in the DEMO design concept shown in Fig. 1, it was decided to start modeling geometric details according to the more advanced design available for the ITER TBM (see Fig. 2).

2. Mathematical manifold model

For determination of pressure distributions along feeding and draining poloidal manifolds of WCLL blankets, a simple model has been derived that couples the flow in manifolds and BUs, and allows calculating flow partitioning among BUs. For unique notation, in the following,
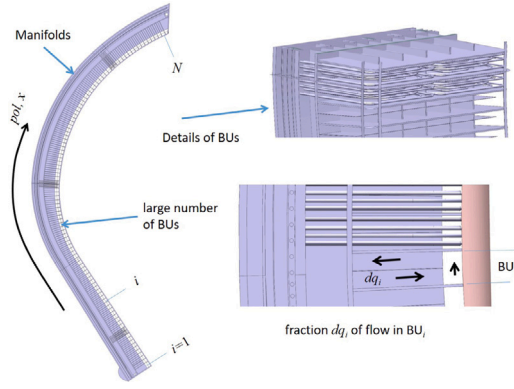

Fig. 1. Design concept of a DEMO blanket segment with a large number N of BUs. A system of manifolds distributes fractions of flow rate dq_i to the breeder units $1 \le i \le N$.
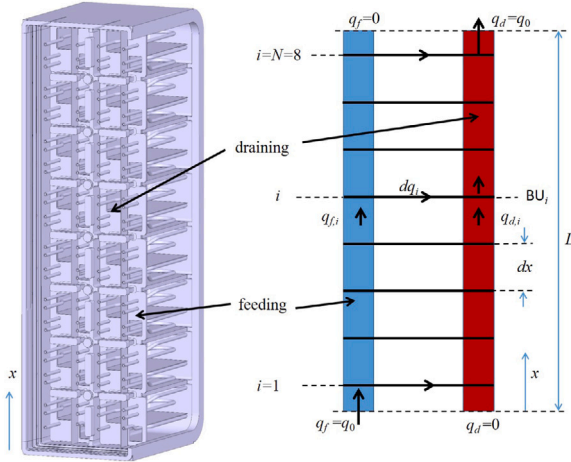

Fig. 2. Design concept of a WCLL blanket module for an ITER TBM with 8 breeder units BUs arranged along the poloidal direction. View into the system of manifolds and sketch defining details of the theoretical model.

subscripts f, d, and BU denote *feeding* and *draining* manifolds, and *breeder units*. The sketch in Fig. 2 shows model definitions for the ITER TBM, but the model is quite flexible and applies for general geometries with a large number of BUs.

The geometry under investigation consists of N BUs of poloidal length dx. For simplifying the analysis we introduce the global nondimensional coordinate $\xi = x/L$, i.e. we measure poloidal position x in fractions of the poloidal length L,

$$x = L\xi, \ dx = L \, d\xi, \ 0 < x < L, \ 0 < \xi < 1. \tag{1}$$

Cross sections of feeding and draining manifolds A_f and A_d are measured as fractions β_f and β_d of the entire manifold cross section $A_M = A_f + A_d$. Cross sections A_{BU} of breeder units are measured as multiples β_{BU} of the same reference area A_M.

$$A_f = A_M \beta_f, \ A_d = A_M \beta_d, \ A_{BU} = A_M \beta_{BU}, \tag{2}$$

where $\beta_f + \beta_d = 1$ and $\beta_{BU} = A_{BU}/A_M$.

The breeder unit i at poloidal position x_i exchanges a part $dq_i = q_0 \, d\alpha_i$ of the total volume flux q_0 between feeding and draining manifolds. After passing position x_i the nondimensional flow rate fractions $\alpha = q/q_0$ in manifolds become

$$\alpha_{f,i+1} = \alpha_{f,i} - d\alpha_i, \tag{3}$$

$$\alpha_{d,i+1} = \alpha_{d,i} + d\alpha_i, \tag{4}$$

where mass conservation requires

$$\alpha_{f,i} + \alpha_{d,i} = 1, \ \sum_{i=1}^{N} d\alpha_i = 1. \tag{5}$$

The local pressure drop in feeding and draining manifolds between position i and $i+1$ can be described as

$$p_{f,i+1} - p_{f,i} = -\sigma B^2 \frac{q_0}{A_M} a \, \Delta p_{f,i}, \tag{6}$$

$$p_{d,i+1} - p_{d,i} = -\sigma B^2 \frac{q_0}{A_M} a \, \Delta p_{d,i}, \tag{7}$$

where Δp_f and Δp_d stand for the magnitudes of nondimensional pressure drops, as functions of $\alpha_{f,i}$ and $\alpha_{d,i}$, in feeding and draining sections of poloidal length dx. The characteristic Hartmann length a is the average value of feeding and draining ducts, it is constant along the poloidal direction for the current TBM design and the mean velocity in manifolds $u_M = q_0/A_M$. The pressure drop in breeder units is

$$p_{f,i} - p_{d,i} = \sigma B^2 \frac{q_0}{A_M} \frac{d\alpha_i}{\beta_{BU}} a_{BU} \, \Delta p_{BU}. \tag{8}$$

Here, $q_0 \, d\alpha_i / A_M \beta_{BU}$ represents the average velocity in a BU, a_{BU} is the Hartmann length of breeder units as available from the design of the TBM mock-up. It is the typical length that is used when the nondimensional pressure drop Δp_{BU} is determined. For complex electrically coupled manifold geometries, Δp_f and Δp_d have to be determined by 3D analyses. An example is described in Section 3.

In nondimensional representation using a pressure scale $p_0 = L \sigma B^2 q_0 / A_M$ and nondimensional pressure $\pi = p/p_0$ we find

$$\pi_{f,i+1} = \pi_{f,i} - \frac{a}{L} \Delta p_{f,i}, \tag{9}$$

$$\pi_{d,i+1} = \pi_{d,i} - \frac{a}{L} \Delta p_{d,i}, \tag{10}$$

$$\pi_{f,i} - \pi_{d,i} = \frac{d\alpha_i}{\beta_{BU}} \frac{a_{BU}}{L} \Delta p_{BU}, \tag{11}$$

where the latter equation is used to determine nondimensional flow rates $d\alpha_i$ in breeder units

$$d\alpha_i = (\pi_{f,i} - \pi_{d,i}) \left(\frac{\Delta p_{BU}}{\beta_{BU}} \frac{a_{BU}}{L} \right)^{-1}. \tag{12}$$

The simulation starts with an initial guess of $d\alpha_i$ satisfying the mass balance (5). Then the pressure distributions in manifolds are determined using (9) and (10), where $\Delta p_{f,i}$ and $\Delta p_{d,i}$ depend on $\alpha_{f,i}$ and $\alpha_{d,i}$, respectively. As entrance conditions we assume a reference pressure $\pi_{f,0} = 0$ and the yet unknown value $\pi_{d,0}$ is determined by an iterative procedure, where all variables are repeatedly updated under the constraint (5).

3. One example: TBM-like manifold geometry

In the following, the model is applied to a geometry that is similar to the WCLL TBM foreseen for ITER (see Fig. 3). One should keep in mind that the present MHD mock-up consists only of a single column of breeder units instead of two as foreseen in ITER and that the coupling with the second column is not taken into account in this study. For the analysis, the manifold is split in a number of unit elements of length dx for which electrically coupled 3D simulations are performed to determine the respective Δp depending on the fraction α of flow rate carried in individual parts. For these simulations a local coordinate system is centered in the middle of the stiffening plates that reduce the manifold cross sections. Although same notation (x) is used here as local poloidal coordinate, one should not be confused with the previously introduced global poloidal coordinate.

Along the poloidal direction, manifold cross sections are constant with periodical constrictions originating from stiffening plates that penetrate the manifold region (see Fig. 3b). The manifolds are separated from each other by a common wall along which both channels are

electrically coupled. Leakage currents may be exchanged across this wall between feeding and draining ducts. A representative manifold element used in scaled mock-up experiments performed in the MEKKA facility at KIT has dimensions of $dx\,(82\,\text{mm}) \times 4a\,(78\,\text{mm}) \times 2d\,(24\,\text{mm})$. Details are shown in Fig. 3b. In the present design [3], the separation wall or so-called baffle plate is shifted by a distance e in y-direction with respect to the middle plane $y = 0$.

To study the influence of electromagnetic coupling by leakage currents at the common wall, the present analysis assumes symmetry with respect to $y = 0$ for simplicity, i.e. we take the baffle plate at $e = 0$. The analysis is performed analogous to [4] using asymptotic methods. This approach applies for strong magnetic fields and neglects inertia effects. This is justified for very strong magnetic fields, i.e. when electromagnetic forces are much larger than inertia forces. The core flow is considered inviscid with viscous corrections in boundary layers. Under these assumptions, the governing equations can be integrated analytically along magnetic field lines and the remaining equations may be solved efficiently in 2D for pressure p and potential ϕ on the fluid–wall interface. The full 3D solution can be reconstructed by analytical relations after p and ϕ are known on the interface. This procedure, initially proposed by Kulikovskii [5], has been implemented in a numerical code using boundary fitted coordinates [6]. The approach has been validated, as described in the latter reference, against analytical solutions for flows in rectangular ducts with aligned and inclined magnetic fields, for circular pipes, and for 3D flows in a sharp backward elbow using experimental data. Further validations have been performed for many other applications such as for instance MHD flows in a sudden expansion [7], where results compare well with full numerical simulations and experiments, even for finite interaction parameters.

For simulations for the mock-up experiments performed in the MEKKA facility at KIT, thermophysical properties are used for the model fluid NaK as $\rho = 863\,\text{kg/m}^3$, $\nu = 9.02 \cdot 10^{-7}\,\text{m}^2/\text{s}$, $\sigma = 2.79 \cdot 10^6\,1/\Omega\text{m}$, [8] and $\sigma_w = 1.24 \cdot 10^6\,1/\Omega\text{m}$ for the wall. In the present work we are mainly interested in fundamental physics effects and therefore we ignore minor details. We consider for instance all walls with the same thickness (an average value) so that all parts have unique wall conductance ratio $c = 0.274$. Here $c = t_w \sigma_w / a\sigma$ describes for thin walls, $t_w \ll a$, the ratio of conductance of the walls and fluid region. The thickness of all walls is assumed $t_w = 12$ mm, except for the thin baffle plate where the major coupling occurs. The thickness of this wall is only 2 mm and its conductance $c = 0.046$.

For these 3D simulations, dimensions are scaled by the mean manifold Hartmann length a (see Fig. 3), and the reference velocity $u_0 = q_0/A_m$ corresponds to the average poloidal velocity in feeding plus draining parts of the manifold, i.e. the mean nondimensional velocity is $\bar{u} = 1$. The nondimensional values Δp denote pressure differences scaled by $\sigma u_0 a B^2$ and ϕ stands for electric potential scaled by $u_0 a B$.

The following results have been obtained for $Ha = 1000$, where the Hartmann number $Ha = aB\sqrt{\sigma/\rho\nu}$ is a nondimensional measure for the strength of the magnetic field. This moderate Hartmann number has been chosen since it allows better visualization of side layer jets in Figs. 4 and 5. For higher Ha, core velocity and pressure drop are quite similar to the ones described for $Ha = 1000$, but since the viscous boundary layers become thinner with increasing Ha, flow features in these regions are more difficult to visualize. Simulations with same pressure differences $\Delta p_f = \Delta p_d$ applied in both manifold ducts, lead obviously to equal flow rates in both channels, i.e. $\alpha_f = \alpha_d = 0.5$. Results for poloidal velocity profiles are displayed in Fig. 4a for a position in the middle ($x = 0$) and at the end of the manifold part ($x = -2.1$). When mean velocities in both ducts are the same, coupling is ineffective and the flows in both channels practically do not interact since no leakage currents are exchanged. As a result, we observe near entrance and exit the typical velocity profiles expected for flows in electrically conducting rectangular ducts, which exhibit uniform core velocity, high-velocity jets in side layers parallel to B
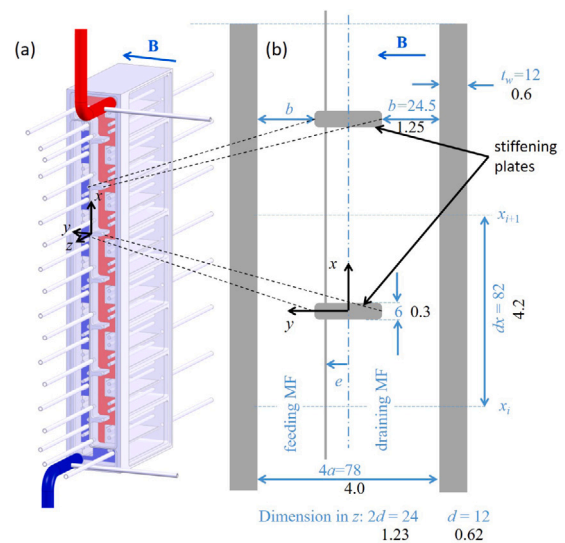

Fig. 3. 3D view of a TBM-like geometry with manifolds and breeder units used for MHD model experiments in the MEKKA facility at KIT (a). Geometry, dimensions and coordinate system in feeding and draining manifolds. Black notation is nondimensional and scaled with a, and the blue one is dimensional and measured in mm (b).
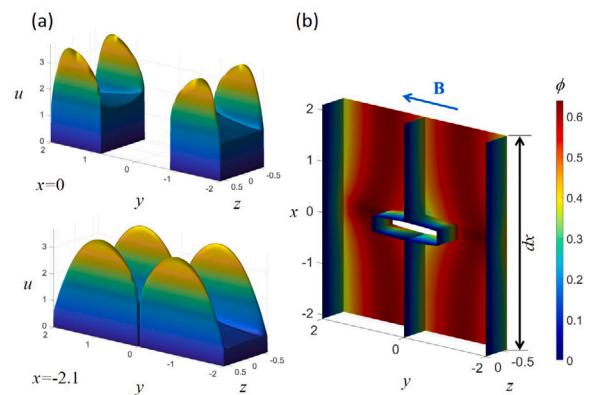

Fig. 4. Results of a simulation with electromagnetic coupling, with same pressure differences in both ducts, $\Delta p_f = \Delta p_d$. (a) Velocity profiles in the symmetry plane $x = 0$ and near the entrance $x = -2.1$, and (b) view on the distribution of nondimensional electric potential on the fluid–wall interface in half of the geometry.

and thin Hartmann layers at walls perpendicular to the magnetic field. When the cross sections become constricted near $x = 0$, the mean velocity increases and the core velocities are no longer constant along y. Some deformation along z is caused by 3D currents near the contraction and expansion at the penetrating stiffening plate. Fig. 4b, shows electric potential on the fluid–wall interface of half the ducts ($z < 0$). One can see that highest values occur along the side walls, in regions where the velocity reaches maximum values. In the other half of the ducts ($z > 0$), not shown in the figure, the distribution is symmetric with $\phi(z) = -\phi(-z)$.

Fig. 5 shows an example where the pressure difference Δp_d along the draining manifold is significantly smaller than in the feeding part $\Delta p_d/\Delta p_f = 0.125$. As a result the fraction of flow in the draining channel decreases and the one in the feeding part increases such that $\alpha_d = 0.313$ and $\alpha_f = 0.687$, i.e. $\alpha_d/\alpha_f = 0.456$. We observe that the ratios of pressure drops and flow rates are not comparable. The reason for this behavior is the electromagnetic coupling where the faster flow in the feeding part pulls the slower flow in the draining duct in the same direction. This leads to increased pressure drop in the feeding channel and reduced pressure drop in the draining one as shown in Fig. 6.
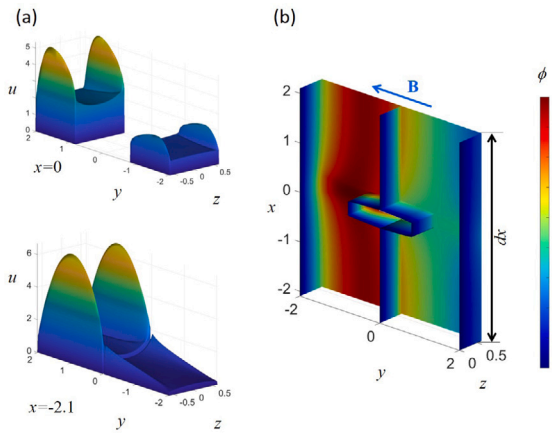
Fig. 5. Results of a simulation with electromagnetic coupling, for pressure differences $\Delta p_d = 0.125\,\Delta p_f$. (a) Velocity profiles in the symmetry plane $x = 0$ and near the entrance $x = -2.1$, and (b) view on the distribution of nondimensional electric potential on the fluid–wall interface in half of the geometry.
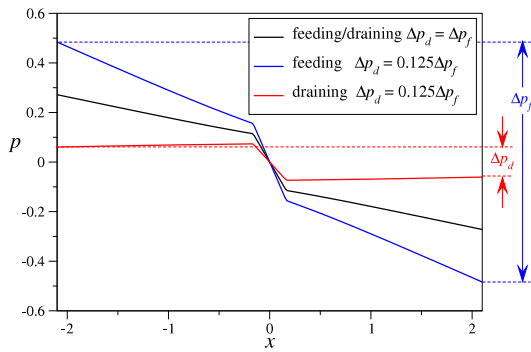

Fig. 6. Pressure distribution in a periodic fraction of the coupled manifolds along the scaled poloidal coordinate for pressure differences $\Delta p_d = \Delta p_f$ (black) and $\Delta p_d = 0.125\,\Delta p_f$ (blue and red).

Fig. 7. Variation of pressure drops Δp_f and Δp_d with flow rate fraction $\alpha_f = 1 - \alpha_d$. Data displayed by symbols has been obtained by coupled 3D analyses of periodic manifold fractions, dashed lines represent best linear fits.

Fig. 8. Distribution of flow rates among 8 BUs in a WCLL TBM mock-up; initial condition and converged solution.

Pressure distributions in the center of feeding and draining ducts are plotted in Fig. 6, where the reference pressure $p = 0$ has been selected in the center at $x = 0$. We observe almost uniform pressure gradients in both manifolds with locally increased pressure drop near constrictions of cross sections (near the stiffening plate). When feeding and draining manifolds carry same flow rates $\alpha_f = \alpha_d = 0.5$, the pressure differences in both parts are equal (black line). However, when the pressure difference in the draining duct is reduced to $\Delta p_d = 0.125\,\Delta p_f$, solutions in feeding and draining ducts differ from each other. Differences Δp_f and Δp_d between entrance an exit are a result of these simulations and their values depending on α_f and α_d are required for the global solution procedure (9)–(10).

For making use of these results in the manifold model described above, it is required to determine Δp depending on α. Results for a large number of 3D simulations are summarized in Fig. 7. The good news is that over a wide range of α values, the pressure drops scale linearly with this quantity. We find by linear fits (dashed lines in Fig. 7)

$$\Delta p_f = 0.544 + 2.263\left(\alpha_f - 0.5\right),\qquad(13)$$

$$\Delta p_d = 0.544 + 2.263\left(\alpha_d - 0.5\right),\qquad(14)$$

i.e. both pressure drops depend in the same way on their respective fraction of flow rate. This results from the assumption that both parts of the manifold have same toroidal dimension for the assumed symmetric case with $e = 0$.
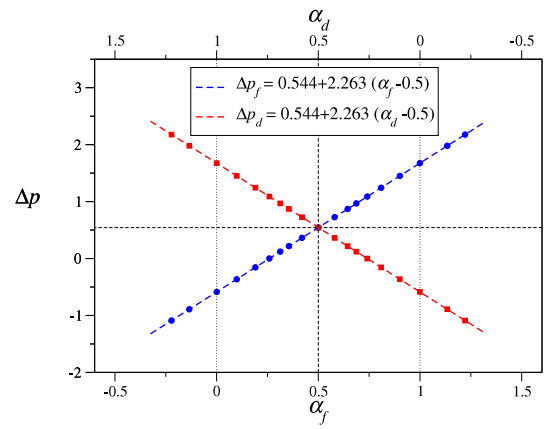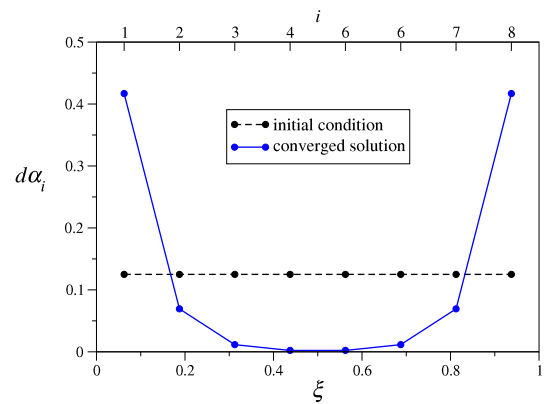
4. Coupling of manifolds with breeder units

The simulation for the entire manifold starts with assumed uniform initial distribution of flow rates in BUs where $d\alpha_i = 1/N$ with $N = 8$ for the present TBM-like example as shown in Fig. 8 by the dashed line. Fig. 9 shows converged results of pressure drops in feeding and draining manifolds according to Eqs. (9) and (10) with (12). It can be seen that in the feeding manifold the pressure drop is the highest for small ξ since here the flow rate is large. Moreover, due to electromagnetic coupling, the flow in the feeding channel pulls fluid in the draining duct where a pressure increase can be observed for the first unit element. The situation is reversed close to the end of the module when approaching $\xi = 1$. Here we have the highest flux in the draining duct with corresponding high pressure drop, while the pressure gradient in the feeding channel is reversed due to coupling by leakage currents. For simplicity, data points between two poloidal positions ξ_i and ξ_{i+1} are connected by straight lines. When resolving the detailed pressure distribution along the poloidal direction one can observe of course the steps caused by additional pressure drop at the local contractions of the cross sections (see e.g. Fig. 4 for details).

Results shown in Fig. 9 correspond to those published in [9]. In the latter reference the distance between feeding and draining pressure distributions $(\pi_{d,0})$ remained undetermined, while now it is prescribed under the constraint of mass conservation. Even if not explicitly shown in Fig. 9, the additional pressure drops near the contractions/expansions are included in the present analysis. In Fig. 9 it can be seen that the driving pressure heads for BUs $i = 3, 4, 5, 6$
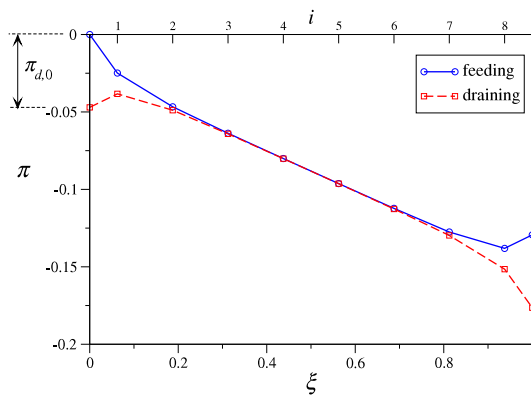
Fig. 9. Pressure distribution in feeding and draining manifolds in a WCLL TBM mock-up obtained eventually when iterative solutions fully converged. The related distribution of flow rates in BUs corresponds to the solid blue line in Fig. 8.

become very small so that the flow rates in these elements practically become insignificant. The latter fact can be observed in Fig. 8 (blue solid line), where the highest flow rates in BUs occur near the ends of the blanket module. Similar conclusions have been reached from previous experimental and numerical analyses for MHD flows in a HCLL blanket module [2].

5. Conclusions

The present work attempts at quantifying MHD pressure drop in feeding and draining manifolds of a model geometry for a WCLL TBM and to determine the flow partitioning in BUs. The manifold is split along the poloidal direction into generic unit elements that are considered in detailed 3D numerical analyses. In the latter simulations, full electric coupling of neighboring feeding and draining channels is taken into account as well as geometric constraints caused by stiffening plates that penetrate the manifolds. Results of 3D simulations are used as input to construct a global solution to the problem. The derived model has been first applied to the case with 8 BUs, where feeding and draining manifold ducts have equal cross sections, i.e. where the dividing baffle plate is in the center of the geometry ($e = 0$). This example has been used to develop an understanding of the main physical effects and to verify if certain symmetries in the solution are met in order to test the correct implementation of the model equations.

In future work, the position of the baffle plate will been taken in an asymmetric way as foreseen in the WCLL TBM design [3], which will then allow comparison with results obtained by a systems code analysis [10]. Moreover, the model will be further applied in future studies to optimize the position of the baffle plate such that flow rates in all BUs become equal in order to give recommendations for modifications to the WCLL TBM design team. The derived model is very flexible and allows efficient and fast determination of the electrically coupled MHD performance of given design concepts with large numbers of BUs as foreseen in DEMO. The main computational effort lies here in the determination of data for pressure drop correlations (as shown e.g. in Fig. 7) by using electrically coupled 3D asymptotic analyses.

In order to determine Δp_f and Δp_d for a specific value of α, a typical simulation run with 140 grid points in axial direction (the magnetic field direction is treated analytically, no numerical resolution) and 40 transverse points in half of a cross section of each manifold requires about 8–9 min on a single CPU of a standard office PC. With some of these simulations, the pressure drop correlations are known and the iterative solution of Eqs. (9) and (10) is then obtained within seconds. Results for poloidal pressure distributions in TBM-like feeding and draining blanket manifolds for $N = 100$ BUs are possible and will be presented in future papers.

Declaration of competing interest

The authors declare that they have no known competing financial interests or personal relationships that could have appeared to influence the work reported in this paper.

Data availability

The authors do not have permission to share data.

References

[1] L. Bühler, C. Mistrangelo, H.-J. Brinkmann, C. Koehly, Pressure distribution in MHD flows in an experimental test-section for a HCLL blanket, Fusion Eng. Des. 127 (2018) 168–172, http://dx.doi.org/10.1016/j.fusengdes.2018.01.007.

[2] C. Mistrangelo, L. Bühler, Determination of multichannel MHD velocity profiles from wall-potential measurements and numerical simulations, Fusion Eng. Des. 130 (2018) 137–141, http://dx.doi.org/10.1016/j.fusengdes.2018.03.041.

[3] J. Aubert, G. Aiello, D. Alonso, T. Batal, R. Boullon, S. Burles, B. Cantone, F. Cismondi, A. Del Nevo, L. Maqueda, A. Morin, E. Rodríguez, F. Rueda, M. Soldaini, J. Vallory, Design and preliminary analyses of the new water cooled lithium lead tbm for iter, Fusion Eng. Des. 160 (2020) 111921, http://dx.doi.org/10.1016/j.fusengdes.2020.111921.

[4] L. Bühler, C. Mistrangelo, Theoretical studies of MHD flows in support to HCLL design, Fusion Eng. Des. 109–111 (2016) 1609–1613, http://dx.doi.org/10.1016/j.fusengdes.2015.11.010.

[5] A.G. Kulikovskii, Slow steady flows of a conducting fluid at large Hartmann numbers, Fluid Dyn. 3 (1) (1968) 1–5.

[6] L. Bühler, Magnetohydrodynamic flows in abitrary geometries in strong, nonuniform magnetic fields, Fusion Technol. 27 (1995) 3–24.

[7] L. Bühler, Three-Dimensional Liquid Metal Flows in Strong Magnetic Fields, Tech. Rep. FZKA 7412, Forschungszentrum Karlsruhe, Habilitation, Universität Karlsruhe, 2008, http://dx.doi.org/10.5445/IR/1000008908.

[8] O.J. Foust, Sodium - NaK Engineering Handbook, Gordon and Breach Science Publishers, New York, London, Paris, 1972.

[9] C. Mistrangelo, L. Bühler, C. Koehly, I. Ricapito, Magnetohydrodynamic velocity and pressure drop in manifolds of a WCLL TBM, Nucl. Fusion 61 (2021) 096037, http://dx.doi.org/10.1088/1741-4326/ac18dc.

[10] L. Melchiorri, V. Narcisi, C. Ciurluini, F. Giannetti, G. Caruso, A. Tassone, Preliminary MHD pressure drop analysis for the prototypical WCLL TBM with RELAP5/MOD3.3, Fusion Eng. Des. 176 (2022) 113048, http://dx.doi.org/10.1016/j.fusengdes.2022.113048.